AAAS
Ultrafast Science
Volume 2022, Article ID 9858739, 9 pages
https://doi.org/10.34133/2022/9858739

Ultrafast Science
A SCIENCE PARTNER JOURNAL

Research Article

Attosecond Optical and Ramsey-Type Interferometry by Postgeneration Splitting of Harmonic Pulse

Takuya Matsubara,[1,2] **Yasuo Nabekawa**,[1] **Kenichi L. Ishikawa**,[3,4,5] **Kaoru Yamanouchi**,[2] **and Katsumi Midorikawa**[1]

[1]*Attosecond Science Research Team, RIKEN Center for Advanced Photonics, 2-1 Hirosawa, Wako-shi, Saitama 351-0198, Japan*
[2]*Department of Chemistry, School of Science, The University of Tokyo, 7-3-1 Hongo, Bunkyo-ku, Tokyo 113-0033, Japan*
[3]*Department of Nuclear Engineering and Management, Graduate School of Engineering, The University of Tokyo, 7-3-1 Hongo, Bunkyo-ku, Tokyo 113-8656, Japan*
[4]*Photon Science Center, Graduate School of Engineering, The University of Tokyo, 7-3-1 Hongo, Bunkyo-ku, Tokyo 113-8656, Japan*
[5]*Research Institute for Photon Science and Laser Technology, The University of Tokyo, 7-3-1 Hongo, Bunkyo-ku, Tokyo 113-0033, Japan*

Correspondence should be addressed to Yasuo Nabekawa; nabekawa@riken.jp

Received 2 May 2022; Accepted 1 June 2022; Published 24 June 2022

Time domain Ramsey-type interferometry is useful for investigating spectroscopic information of quantum states in atoms and molecules. The energy range of the quantum states to be observed with this scheme has now reached more than 20 eV by resolving the interference fringes with a period of a few hundred attoseconds. This attosecond Ramsey-type interferometry requires the irradiation of a coherent pair of extreme ultraviolet (XUV) light pulses, while all the methods used to deliver the coherent XUV pulse pair until now have relied on the division of the source of an XUV pulse in two before the generation. In this paper, we report on a novel technique to perform attosecond Ramsey-type interferometry by splitting an XUV high-order harmonic (HH) pulse of a sub-20 fs laser pulse after its generation. By virtue of the postgeneration splitting of the HH pulse, we demonstrated that the optical interference emerging at the complete temporal overlap of the HH pulse pair seamlessly continued to the Ramsey-type electronic interference in a helium atom. This technique is applicable for studying the femtosecond dephasing dynamics of electronic wavepackets and exploring the ultrafast evolution of a cationic system entangled with an ionized electron with sub-20 fs resolution.

1. Introduction

The interference of wavefunctions to describe the probability amplitudes of quantum states, such as electronic states of atoms and molecules, originates from the coherence of ultrashort optical pulses used for generating such states, and the coherence of wavefunctions lies at the heart of a variety of research fields in ultrafast atomic and molecular science [1–3]. For example, a coherent superposition of vibrational states in a molecule, which can typically be formed by the irradiation of a femtosecond laser pulse, is called a vibrational wavepacket [4, 5]. Even though the averaged position of a vibrational wavepacket should evolve in accordance with classical vibrational motion, the wave characteristic of a vibrational wavepacket emerges as the stretch and shrink of its spatial distribution upon time evolution, which is governed by the interference of the vibrational wavefunctions involved. The interference of vibrational wavepackets also plays an essential role in the wavepacket interferometry used to study fundamental physics and its applications to controlling chemical reactions [6, 7]. We note that wavepacket interferometry relies on the stable generation of a pair of coherent femtosecond pulses to generate a pair of vibrational wavepackets that interfere with each other.

Regarding the time scale of vibrational wavepacket dynamics, a typical period of a molecular vibration is longer than 10 fs, because vibrational wavefunctions with adjacent energy separations of less than 0.4 eV (≃100 THz) are usually superposed. The time scale of a wavepacket can drastically decrease to a sub-fs range when the wavefunctions of

electronic states in an atom or a molecule with energy separations of more than 5 eV are coherently superposed to form an electronic wavepacket, as was reported in refs. [8–10]. The period of the time evolution of the superposition of the electronic ground and excited states of atoms and molecules is typically of the order of a few hundred attoseconds, reflecting the large energy separation. Under this situation, the wavepacket at time t should be expressed as a linear combination of the electronic ground state and excited state vectors, $|g\rangle$ and $|e\rangle$, as $|\psi(t)\rangle = a|e\rangle e^{-i\Delta Et/\hbar} + b|g\rangle$, where the energy difference between the ground and excited states is denoted as ΔE and $\hbar$ is Planck's constant divided by 2π. The irradiation of an optical pulse with a photon energy of ΔE at time $t = 0$ is the simplest method to generate such an electronic wavepacket, because $|e\rangle$ should be generated from the one-photon transition from $|g\rangle$. By irradiating a second optical pulse coherent with the first pulse after the time delay Δt_{ctrl}, the wavepacket may be described as $|\psi(t, \Delta t_{\mathrm{ctrl}})\rangle = a|e\rangle e^{-i\Delta Et/\hbar} + a'|e\rangle e^{-i\Delta E(t-\Delta t_{\mathrm{ctrl}})/\hbar} + b'|g\rangle$ only if we can assume the coherence between $|g\rangle$ and $|e\rangle$. The probability of finding the wavepacket to be in the excited state, p_e, should be proportional to $|\langle e|\psi(t, \Delta t_{\mathrm{ctrl}})\rangle|^2_{t\longrightarrow\infty} = |a|^2 + |a'|^2 + 2\Re\{aa'^* e^{i\Delta E\Delta t_{\mathrm{ctrl}}/\hbar}\}$, and thus, we can identify the electronic wavepacket by observing that the population of the excited state is modulated with a period of $2\pi\hbar/\Delta E$ upon scanning the delay Δt_{ctrl}. This type of interferometry of quantum states is called Ramsey-type interferometry in the time domain.

To demonstrate a quantum beat with a period of a few hundred attoseconds in Ramsey-type interferometry, the energy difference ΔE should be much larger than 10 eV, which is equivalent to the photon energy of an optical pulse in the extreme ultraviolet (XUV) wavelength region. Therefore, the main issue in performing the attosecond Ramsey-type interferometry is how to generate a coherent pulse pair in the XUV region, although it is very difficult to fabricate a half mirror in this wavelength region.

One of the practical solutions for this issue is the temporal division of a source of an XUV pulse. Cavalieri and coworkers devised a scheme to generate a pair of coherent XUV high-order harmonic (HH) pulses with a duration of a 100 fs, in which they made the two replicas of fundamental laser pulse in the near-infrared (NIR) wavelength region by using a conventional Michelson-type interferometer [11–13]. They focused these two replicas of the fundamental laser pulse into a xenon gas target to generate an XUV HH pulse pair, which was applied to time-domain Ramsey-type interferometry to achieve high-resolution spectroscopy. Recently, this time-domain Ramsey-type interferometry was applied to the Rydberg states of He atoms by Koll and coworkers [14]. Two replicas of phase-locked fundamental laser pulse can also be generated using an optical parametric amplifier (OPCPA) system seeded by a frequency-comb laser whose frequency is locked to an atomic clock. Dreissen and coworkers [15] obtained high-resolution spectra of Xe atoms using the seventh harmonic of the NIR pulse pair delivered from this type of OPCPA system.

Attosecond Ramsey-type interferometry exploiting the XUV pulse pair generated from the divided source has also been developed using other types of XUV light sources. Wituschek et al. adopted a Mach–Zehnder-type interferometer (MZI) to split a 100 fs ultraviolet (UV) femtosecond pulse to deliver a pair of fundamental seed pulses to an X-ray free electron laser (XFEL), in which an XUV harmonic pulse pair emerged [16, 17]. They realized a long range of delay scanning reaching nearly 10 ps with the aid of a phase cycling method, resulting in high-precision spectroscopy for the atomic transition lines in the XUV regime. Hikosaka et al. developed tandem undulators to make a relativistic electron emit a pair of XUV pulses in the storage ring of a synchrotron orbital radiation (SOR) facility [18, 19]. The delay between the XUV pulses was adjusted by using a phase shifter for the relativistic electron placed between the tandem undulators. They successfully performed a delay scan up to the ~10 fs range to obtain Ramsey-type interference fringes in their studies on He and Xe atoms originating from the coherence between two XUV wavepackets with a duration of ~2 fs, even though many pairs of XUV pulses (~10^9) were randomly distributed within an entire pulse having a duration of 300 ps.

One promising application of attosecond Ramsey-type interferometry is the investigation of the electronic wavepacket in a molecule having nuclear degrees of freedom. As has been reported by Kobayashi et al. [20], in the transient XUV spectroscopy of Br_2^+, the coherence in the electronic wavepacket in a molecule created by an ultrashort laser pulse can be altered by the vibrational motion. Direct observation of ultrafast motion of an electronic/nuclear wavepacket cannot be implemented with conventional frequency-domain spectroscopy, and thus, it should be considered as a benefit of the attosecond Ramsey-type interferometry. In order to explore the temporal evolution of such an attosecond electronic wavepacket influenced by femtosecond vibrational wavepackets by means of Ramsey-type interferometry, the temporal separation between the two XUV pulses should be as small as tens of femtoseconds.

However, if we divide an NIR pulse into two before high-order harmonics generation (HHG), the temporal separation between the resulting two XUV pulses cannot be sufficiently small, because the interference of the two NIR pulses causes a complex modulation of the XUV intensity. For example, the interference signal in [14] exhibits such modulations in the delay time range shorter than ~50 fs due to the interference of the NIR pulses and their pedestals. In addition, at the higher NIR intensity, the variations of the density and the density distribution in the nonlinear medium perturbed by the first NIR pulse for HHG cannot be revived before the arrival of the second NIR pulse for HHG. It has also been reported that the minimum temporal separation achieved using a seeded XFEL light source [17] cannot be shorter than ~100 fs owing to the interference of the seed pulses in the generation of the XUV pulses.

In this work, we performed time-domain Ramsey-type interferometry using a coherent XUV HH pulse pair created by a split-and-delay interferometer [21] set behind a target gas cell for generating the HH pulse. Our idea for revealing the optical and Ramsey-type interferences was to selectively ionize target atoms (helium (He) atoms were chosen as a proof of principle target) in a region where the loosely

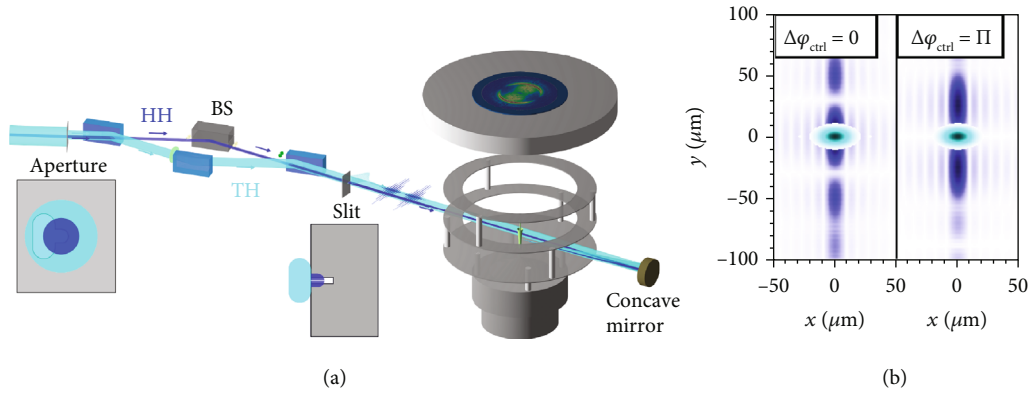

FIGURE 1: Experimental setup. (a) Pump-control-probe interferometer is followed by velocity map imaging spectrometer of electrons. Blue and cyan lines represent the HH and TH beam paths, respectively. The schematic figures of the aperture and the slit before and after the interferometer, respectively, are also shown. (b) Left: the simulated spatial profiles of the 13th HH pulse at $\Delta\varphi_{\mathrm{ctrl}} = 0$ and that of the TH pulse on the focal plane are shown as image plots in blue and cyan, respectively. Right: the simulated spatial profiles at $\Delta\varphi_{\mathrm{ctrl}} = \pi$. The x axis is parallel to the direction of the slit inserted in the beam path of the HH pulse.

focused XUV HH pulse pair spatially interfere and excite the target atoms by irradiating them with a tightly focused 3rd harmonic (TH) UV pulse. Thanks to the high-photon energy of the UV pulse, we can probe the population in the 1s2p (^{1}P) excited state by the photoionization, which cannot be induced by the NIR probe pulse adopted previously in other schemes [11, 12, 14]. By taking advantage of the postgeneration splitting of the HH pulse, we were able to observe that the fringes in the electron yield originating from the optical interference of the HH pulse pair with a period of ~200 as around $\Delta t_{\mathrm{ctrl}} \simeq 0$ seamlessly continued to the time-domain Ramsey-type fringes originating from the quantum interference around $\Delta t_{\mathrm{ctrl}} \geq 10$ fs. We have already demonstrated that the pulse durations of the HH and UV pulses can be shortened to less than 10 fs [22], and thus, our novel experimental setup will be feasible to unveil the sub-20 fs dynamics of a nuclear wavepacket with the modulations of Ramsey-type fringes and also to investigate the entanglement of electrons and nuclei in an ionized molecule [23, 24] as recently demonstrated [25].

2. Materials and Methods

2.1. XUV HH Beamline. We utilized a laboratory-built chirped-pulse amplification (CPA) system of a Ti:sapphire laser [26] to deliver the fundamental (NIR) laser pulse at a repetition rate of 100 Hz. A regenerative amplifier at the first stage in the amplifier chain of the CPA system contained two plates with dielectric coatings, which we call gain narrowing compensators (GNCs), in a cavity to compensate for the gain narrowing of the spectrum, such that the spectral width could be sufficiently broad to form a 12 fs pulse at the shortest. In the experiment reported in this paper, the incident angle to the GNCs was adjusted to tune the peak wavelength of the amplified pulse to ~780 nm at the expense of the narrowing of the spectral width. The pulse duration and energy were estimated to be ~18 fs and ~20 mJ, respectively.

The HH pulses were generated by focusing the NIR pulses into a gas cell filled with Xe by using a concave mirror with a focal length of 5 m. The wavelengths of the HH pulses were tuned so that the photon energy of the 13th HH pulse coincided with the energy difference between the 1s^2 ground state and the 1s2p (^{1}P) excited state in He by adjusting the intensity of the NIR pulses with an aperture set behind a grating-pair compressor in the CPA system. The HH wavelength was tuned by the blue shift caused by the rapid change in the induced dipole phase in a Xe atom at the leading edge of the NIR pulse in the HH generation process [27]. The phase matching conditions for the 13th HH pulse were still maintained even after the tuning of the HH wavelength. This is probably because we adjusted the pressure of the Xe gas to be 30–50% higher than the typical pressure for the compensation of the decrease of neutral Xe atoms upon the ionization. We made use of the TH pulse simultaneously generated and copropagating with the HH pulse as the probe pulse. This is advantageous compared with the TH pulse generation in a separated beam path of the NIR pulse because we did not need an active delay stabilization technique required for the large scale interferometer with arm lengths of more than a few meters [28]. The phase matching conditions for the TH generation were not achieved, but the intensity of the TH pulse was sufficiently high to ionize He in the 1s2p (^{1}P) state.

The HH pulse and the TH pulse generated from a xenon gas target encountered a specially designed front aperture set ~4 m downstream from the xenon gas cell, as shown in Figure 1. The beam profile of the HH pulse mainly passed through the central hole (2 mm diameter) of the aperture owing to the small divergence of the HH pulse, while the side area in the beam profile of the TH pulse, which exhibited divergence much larger than that of the HH pulse, was transmitted to an oval hole with major and minor axes of 8 mm and 4 mm, respectively, placed beside the central hole of the aperture. The central area of the TH pulse also propagated through the central hole with the HH pulse. The front aperture eliminated part of the intense fundamental NIR

pulse to relax the thermal load of the optical elements absorbing the NIR pulse in the hybrid interferometer. The front aperture also excluded the HH field components originating from the so-called long-trajectory electrons, which might appear as a halo around the central HH pulse emerging from the short-trajectory electrons under the phase-matching condition with the NIR pulse, even though the intensity of the halo was expected to be negligibly low due to the phase-mismatch [29].

In the downstream of the front aperture, the HH pulse was reflected just above and below the horizontal boundaries of two Si plate beam splitter (SiBS) mirrors situated as closely as possible, by which the HH pulse was split spatially into two replicas. The NIR pulse was significantly reduced upon this reflection because the incident angle was set to be the Brewster angle of the NIR wavelength (75°). As a result, the intensity of the NIR pulse was sufficiently low to avoid the two-color above-threshold ionization (ATI) by absorbing an NIR photon in addition to an HH photon. We adjusted the delay Δt_{ctrl} by translating the lower SiBS mirror with a piezo actuator.

On the other hand, the side area in the beam profile of the TH pulse was reflected by a dichroic mirror placed between the front aperture and the SiBS mirrors and then sent to a second dichroic mirror to configure an MZI with a third dichroic mirror. The UV TH pulse reflected by the third dichroic mirror copropagated to the side of the two replicas of the HH pulse. The dielectric coating on the dichroic mirrors was designed to have a reflectivity of more than 90% in the wavelength region of the TH pulse and less than 4% in the wavelength region of the NIR pulse. The pulse energy of the NIR pulse was reduced to less than 10^{-4} as a result of reflections with three dichroic mirrors composing the MZI, so that we could exclude the nonlinear effects of the NIR pulse such as two-color ATI with HH pulses. The time delay of the TH pulse with respect to the first replica of the HH pulse, Δt_{prb}, can be controlled by positioning the third dichroic mirror set on a translation stage driven by a piezo actuator. We adjusted the position of the third dichroic mirror so that the side edge of the mirror did not clip the beam edge of the HH pulse pair reflected by the two SiBS mirrors even at the negative delay of $\Delta t_{\mathrm{prb}} \sim -40$ fs, while the reflection of the TH pulse at the third dichroic mirror clipped slightly the side edge of the TH pulse at the positive delay of $\Delta t_{\mathrm{prb}} \sim 100$ fs. Because the HH pulse still remains in the side area in the beam profile used for the TH pulse even after the three reflections on the dichroic mirrors, we placed a quartz plate with a thickness of 42 μm between the first and second dichroic mirrors to completely remove it. The pulse duration of the TH pulse was estimated to be ~ 11 fs from the measured spectrum and the dispersions of the quartz plate and dichroic mirrors. The pulse duration was reduced to sub-10 fs [30] when we maximized the spectral width of the NIR pulse by adjusting the GNCs.

We inserted a horizontal slit with a width of 500 μm only in the beam path of the HH pulse pair to restrict the areas of the beam profiles reflected near the horizontal boundaries of the two Si plate mirrors. The HH pulse pair and the TH pulse were passed once a velocity map imaging (VMI) spectrometer for electrons and were reflected back and focused by a SiC concave mirror with a radius of curvature of 600 mm. The crossing angle between the HH pulses and the TH pulse was ~ 0.01 rad. We adjusted the focal point so that it was located in a gas jet of He, which was injected through the central pinhole of the repeller plate electrode in the VMI, while the incident pulses before the reflection by the SiC concave mirror passed ~ 10 mm away from the gas jet to reduce the photoionization of He with the incident 15th and higher-order HH pulse pairs.

We show the simulated spatial profile of the TH pulse and that of the 13th HH pulse pair at the focal point in Figure 1(b) to explain why we can observe the interference fringes. Δt_{ctrl} was assumed to be close to 0 fs. When Δt_{ctrl} is equal to 0, the 13th HH pulse pair constructively interferes and exhibits a hump at the center of the spatial profile, as depicted with a blue image in the left panel of Figure 1(b). The valley gradually moves to the center upon changing $\Delta\varphi_{\mathrm{ctrl}} \equiv \omega_{13}\Delta t_{\mathrm{ctrl}}$ and arrives at the center when $\Delta\varphi_{\mathrm{ctrl}}$ was adjusted to π owing to the destructive interference of the 13th HH pulse pair, as depicted with a blue image in the right panel of Figure 1(b), where ω_{13} represents the angular frequency of the 13th HH pulse pair tuned to $\Delta E_{2p}/\hbar$. The TH pulse can exclusively ionize He atoms in the central region of the spatial interference fringe of the two pulses in the HH pulse pair because the vertical width of the spatial profile of the 13th HH pulse pair is much larger than that of the UV pulse, as depicted with a cyan image in both panels in Figure 1(b), owing to the vertically narrow HH profile clipped by the horizontal slit before the focusing. The position-dependent phase relationship between the two HH pulses and thus the fringe amplitude on the photoionization signal should remain the same even when Δt_{ctrl} becomes sufficiently large for the HH pulses to be temporally separated.

2.2. Retrieval of Photoelectron Spectra. Photoelectrons ejected from He are recorded by a position sensitive detector composed of two microchannel plates with chevron stacking, a phosphor screen, and a CMOS camera recording fluorescent images. We performed the counting analysis of the fluorescent spots in each recorded image, and the counting images at the same Δt_{ctrl} step in every scanning were summed. In the resultant counting images, the signal of the 1s2p electrons appeared on the huge background signal of electrons, which originated from the photoionization of residual He atoms in the beam path of the unfocused HH pulses passing ~ 10 mm away from the He beam. We could record only the background electrons by shifting the trigger of the pulsed gas valve so that the gas jet should be injected immediately after the HH pulses passed the focal region. This background electron signal image was used to fit the signal image area of the background electrons around that of the 1s2p electrons to compensate for the fluctuation and inhomogeneity of the background electrons. The net signal image of the 1s2p electrons was obtained by subtracting the fitted signal image of the background electrons.

3. Results

3.1. Photoelectron Spectra. We show the angularly resolved image of electrons measured using the VMI spectrometer in Figure 2. To obtain the image in this figure from the recorded image, we removed intense unwanted electron signals originating from the background He atoms and other residual molecules, which were ionized in the volume of the first propagation path of the HH pulse before it was focused with the SiC concave mirror. The images recorded in the range of Δt_{ctrl} from −0.5 to 14.5 fs were summed, and Δt_{prb} was fixed to 184 fs during the image recordings.

First, we assumed that the two most intense crescent-shaped images in this figure were the electron spectrum arising from the 1s2p excited state ionized with one photon of the TH pulse because the kinetic energy (KE) of ~1.5 eV coincided with that expected from the energy diagram shown in Figure 3(a). This assumption was verified by the observation that this electron spectrum disappeared when the 13th HH spectrum was detuned.

Next, we measured the evolution of the electron yield in this spectral range as a function of Δt_{prb} as shown in Figure 4. The spectrum at each Δt_{prb} step was normalized by the signal intensity of the electrons integrated in the KE range from 2.8 to 3.2 eV, which originating from the one-photon absorption of the 17th HH pulse, to compensate for the fluctuation of the laser intensity. This normalization was performed before the subtraction of the signal image of the background electrons. The yield of 1.5 eV KE electrons rises at around $\Delta t_{\mathrm{prb}} \geq 0$. We evaluated the rise time T_{rise} by fitting the electron yield to the function of $I_0 + I[1 + \mathrm{erf}(\Delta t_{\mathrm{prb}}/T_{\mathrm{rise}})]$, resulting in $T_{\mathrm{rise}} = 16.3 \pm 1.0$ fs, where erf is the error function. We ensured from this measurement that the intensity of the TH contained in the HH pulse pair is too weak to ionize the 1s2p state. This is because the beam profile of the TH contained in the HH pair was ~19 times as large as that of the 13th HH at the focal point.

In addition, the angular distribution of this electron spectrum was different from those of the electron spectra at KEs of ~3 eV and ~0 eV, which were expected to be generated via photoionization from the $1s^2$ ground state by absorbing one photon of the 17th and 15th HH pulses, respectively. The β-parameters, by which the angular distribution of the electron spectrum is represented as $A_0[1 + \beta_2 P_2(\cos\theta) + \beta_4 P_4(\cos\theta)]$, are obtained by pBasex inversion [31], where P_ℓ is the ℓth Legendre polynomial and the angle θ was measured from the p_y axis. The β-parameters are $\{\beta_2, \beta_4\} = \{3.1, 2.5\}$ for the 1.5 eV KE electrons and $\{\beta_2, \beta_4\} = \{2.5, 0.5\}$ and $\{1.0, -0.5\}$ for the 3 eV and 0 eV KE electrons, respectively. The substantial increase in β_4 for the 1.5 eV KE electron spectrum indicates that the distribution is more biased along the polarization direction of the HH and TH pulses. This is evidence that the 1.5 eV KE electrons originate from a multiphoton absorption process. To confirm this, we simulated the photoionization process from the 1s2p state by directly solving the full-dimensional two-electron time-dependent Schrödinger equation (TDSE) [32–35]. The β-parameters $\{\beta_2, \beta_4\} = \{2.686, 2.035\}$ extracted from the simulation agree reasonably well with those obtained experimentally for the 1.5 eV KE electrons.

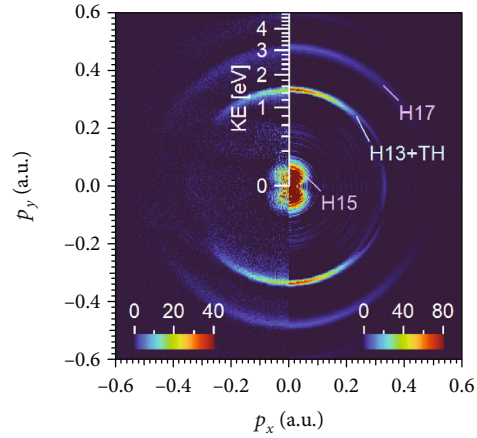

FIGURE 2: Velocity map image of electrons. The left half shows the image after the background subtraction, and the right half shows the image after the pBasex inversion. The two most intense crescent-shaped images represent the angularly resolved spectrum of electrons originating from the 1s2p state of He excited by the 13th HH pulse and then photo-ionized by the TH pulse. The other images, assigned to photoelectron spectra from the ground state with the one-photon absorption of the 15th and 17th HH pulses, are indicated with "H15" and "H17" tags, respectively. The p_x and p_y axes represent the calibrated momenta of electrons in atomic units. An axis signifying the kinetic energy, KE, is also inserted. The polarization directions of the HH and TH pulses are both parallel to p_y.

3.2. Interferometry. We scanned the temporal separation between the HH pulses, Δt_{ctrl}, to find interference fringes appearing in the electron yields from the 1s2p state. The incremental step of Δt_{ctrl} was fixed to 26.6 as to sufficiently resolve the ~200 as period of the interference fringes. The spectrum at each delay of Δt_{ctrl} was normalized by the signal intensity in the KE range from 2.8 to 3.2 eV. We subtracted the background signal in the KE profile at each delay before applying this normalization process. The start time of Δt_{ctrl} was chosen to be slightly negative to ensure that the scanning range included $\Delta t_{\mathrm{ctrl}} = 0$. The total number of incremental steps was 601. As a result, Δt_{ctrl} exceeded the optical coherence time of the 13th HH pulse at the end of the scan. The delay of the TH pulse, Δt_{prb}, was fixed to 184 fs, which was sufficiently long after the irradiation of the second HH pulse. We integrated angularly a net signal image of the electrons to obtain the KE spectrum at each delay of Δt_{ctrl} without using the pBasex inversion in order to prevent the accumulation of the noise in the signal intensities during the inversion process. Figure 5(a) presents the evolution of the angularly integrated KE spectrum of photoelectrons in the range of Δt_{ctrl} from −0.5 to 14.5 fs. In addition to the procedure for deriving the delay-KER spectrogram shown in Figure 5(a), we applied the pBasex inversion method to the total signal image integrated over the

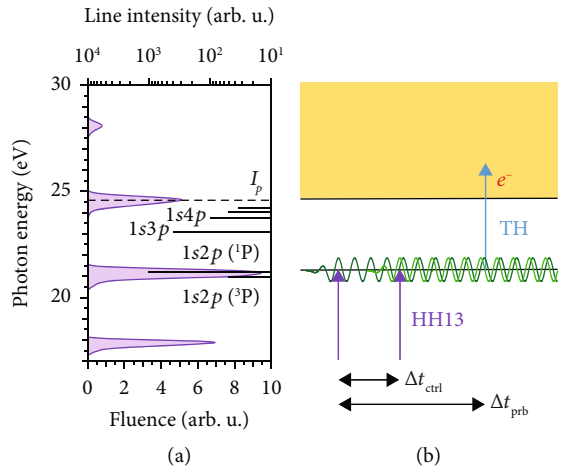

FIGURE 3: Energy diagram and scheme of Ramsey-type interferometry. (a) The solid curve with the shaded area depicts the spectrum of the relative fluence of the XUV HH pulses estimated at the focal point (bottom axis). Horizontal bars represent the intensities of the relevant atomic lines of the He atom (top axis) labeled with the electron configurations of the excited states. The dotted line indicates the ionization energy of the He atom. (b) Scheme of the time-domain Ramsey-type interferometry adopted in this study. The 13th HH pulse pair (purple arrows) with a time separation of Δt_{ctrl} induces two electronic wavepackets composed of the $1s^2$ ground and 1s2p (^{1}P) excited states. The excited state generated by the first 13th HH pulse interferes with that generated by the second 13th HH pulse. The population of the 1s2p (^{1}P) excited state is evaluated from the photoelectron yield with the 3rd harmonic pulse (cyan arrow) irradiated after time delay $\Delta t_{prb}(\gg\Delta t_{ctrl})$ with respect to the first 13th HH pulse.

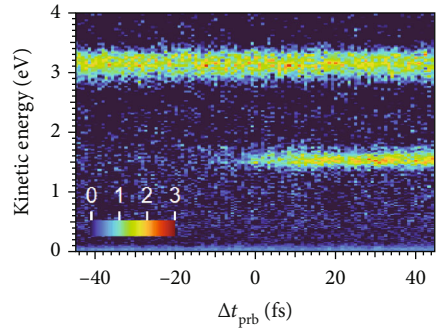

FIGURE 4: Yield of the 1s2p photoelectrons upon scanning Δt_{prb}. The delay between the HH pulses, Δt_{ctrl}, was fixed to 0 in this measurement.

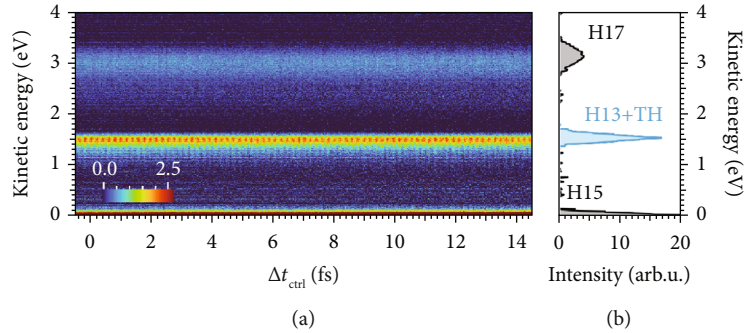

FIGURE 5: Kinetic energy spectrum of electrons. (a) Evolution of kinetic energy (KE) spectrum of electrons upon scanning Δt_{ctrl}. (b) KE spectrum of electrons retrieved from the velocity map image of electrons integrated over Δt_{ctrl} with pBasex method.

entire delay range of Δt_{ctrl} in order to retrieve the sliced image of the photoelectrons as have already been shown in Figure 2. The resultant photoelectron spectrum calculated from the sliced image is shown in Figure 5(b). The sharp peak at ~1.5 eV originating from the ionization by the TH pulse from the 1s2p excited states, which is labeled as H13 + TH, exhibits periodic oscillation in Figure 5(a). This is in contrast to the peak at ~3.2 eV labeled as H17

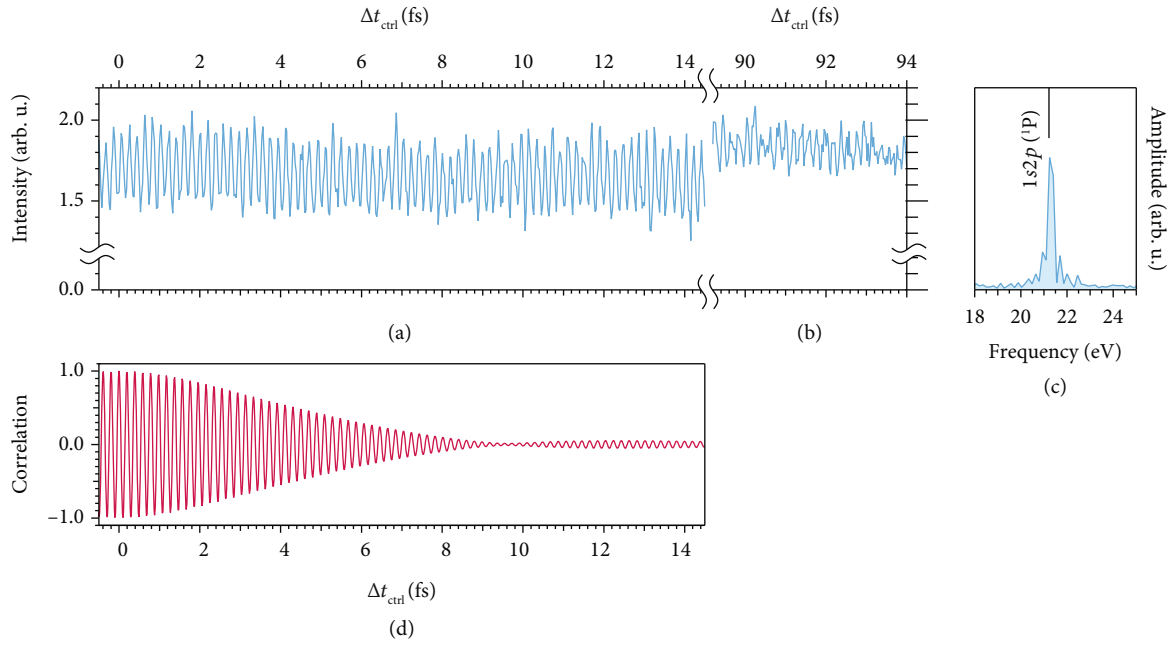

FIGURE 6: Interference fringes. (a) Evolution of the 1s2p (^{1}P) electron yield obtained by integrating the KE spectrum shown in Figure 5(a) from 1.4 to 1.6 eV for each delay step. (b) Evolution of the 1s2p (^{1}P) electron yield in the Δt_{ctrl} range from 89 to 94 fs. (c) Fourier transformed spectrum of the trace shown in (a). The vertical bar represents the energy of the singlet 1s2p atomic line of He. (d) Linear interferometric autocorrelation function of the 13th HH pulse reconstructed from the recorded XUV spectrum shown in Figure 3(a).

and that at ~0 eV labeled as H15, which exhibit no notable intensity modulation.

We integrated the intensity of the H13 + TH peak profile from 1.4 to 1.6 eV to obtain the photoelectron yield and plotted the yield as a function of Δt_{ctrl} in Figure 6(a). The yield exhibits an interference fringe with an oscillation period of ~200 as.

Ramsey-type interference is also observed in the Δt_{ctrl} range from 89 to 94 fs, as depicted in Figure 6(b). The amplitude of the fringes of the trace in Figure 6(b) is, however, only ~30% of that in the Δt_{ctrl} range from −0.5 to 14.5 fs (Figure 6(a)). This degradation can be ascribed to the lateral shift of the delayed 13th HH beam associated with the translation of the SiBS mirror [36].

3.3. Discussion. We performed a Fourier transform of the temporal evolution of the photoelectron yield in Figure 6(a) and obtained the Fourier transformed spectrum shown in Figure 6(c), from which we obtained the frequency of the modulation in Figure 6(a) to be 5.14 PHz, corresponding to an energy separation of 21.2 eV. This energy separation is consistent with the excitation energy of the singlet 1s2p states in He from the ground state [37]. The linewidth of 76 THz is mostly determined by the Δt_{ctrl} range of ~15 fs = $(67\ \mathrm{THz})^{-1}$.

The linear optical interferometric autocorrelation trace calculated from the recorded 13th HH spectrum is shown in Figure 6(d). The amplitude of the oscillation in the measured photoelectron yield in Figure 6(a) does not decrease even after Δt_{ctrl} ~ 10 fs, at which the fringes of the optical interference almost disappear as depicted in Figure 6(d). Therefore, we concluded that the interference fringes appearing in the delay region of $\Delta t_{ctrl} > 10$ fs originated from the Ramsey-type quantum interference. We suppose that the gradual decrease in the visibility of the oscillation originating from the optical interference was compensated for by the gradual increase in the visibility of the oscillation originating from the coexisting Ramsey-type quantum interference upon scanning Δt_{ctrl} from 0 to ~10 fs.

In this work, we successfully observed optical and Ramsey-type interference fringes with a period of ~200 as by using our newly developed device combining a split-and-delay interferometer to generate the HH pulse pair and an MZI to deliver the probe TH pulse. The key feature of this measurement was that we ionized He atoms in only a small part of the region, where the fields of the HH pulse pair spatially interfered with each other, by irradiating the tightly focused TH pulse into this region.

This novel approach should facilitate the investigation of the ultrafast temporal evolution of the coherence between electronic states coupled with nuclear dynamics [20, 38, 39]. In molecules, a superposition of the electronic states can be regarded as a subsystem of the bipartite electronic-vibrational wavepacket. Therefore, the coherence within the electronic states is expected to be detuned, destroyed, and revived by the nuclear dynamics in the respective electronic states. Indeed, our interferometer can access these evolutions by means of Ramsey-type interferometry because the starting time of the delay scan can be arbitrarily small, and the pulse duration of the respective pulses in the pulse pair can be less than 10 fs [22]. In addition, in a similar manner to that proposed in [24] and demonstrated in [25], we can control the entanglement of a photoelectron and a

molecular ion created simultaneously by the photoionization of the molecule by modulating the photoelectron spectrum using a pair of XUV pulses and probing the vibration of the molecular ion using a third pulse in coincidence with the detection of the photoelectron.

Data Availability

Data underlying the results presented in this paper are not publicly available at this time but may be obtained from the authors upon reasonable request.

Conflicts of Interest

The authors declare that there is no conflict of interest regarding the publication of this article.

Authors' Contributions

T. Matsubara performed the experiment, analyzed the data, and wrote the paper. Y. Nabekawa proposed this study; developed the laser system, including the pump-control-probe interferometer; and conducted the experiment. K. L. Ishikawa was involved in the theoretical analysis of the angular distribution of the photoelectrons. K. Yamanouchi supervised the experiment on VMI. K. Midorikawa directed the research in accordance with the Extreme Photonics research project of RIKEN.

Acknowledgments

This work was supported by the Core Research for Evolutional Science and Technology (JPMJCR15N1) of JST, the Center of Innovation Program (JPMJCE1313) of JST, a Grant-in-Aid for Specially Promoted Research (JP15H05696) from MEXT, Grants-in-Aid for Scientific Research (19H00869, 19H05628, 20H00371, 26247068, 20H05670) from MEXT, and the Quantum Leap Flagship Program (JPMXS0118068681, JPMXS0118 067246) of MEXT, Japan.

References

[1] N. F. Scherer, R. J. Carlson, A. Matro et al., "Fluorescence-detected wave packet interferometry: time resolved molecular spectroscopy with sequences of femtosecond phase-locked pulses," *Journal of Chemical Physics*, vol. 95, no. 3, pp. 1487–1511, 1991.

[2] N. Picqué and T. W. Hänsch, "Frequency comb spectroscopy," *Nature Photonics*, vol. 13, no. 3, pp. 146–157, 2019.

[3] R. Blatt and D. Wineland, "Entangled states of trapped atomic ions," *Nature*, vol. 453, no. 7198, pp. 1008–1015, 2008.

[4] D. J. Tannor and S. A. Rice, "Control of selectivity of chemical reaction via control of wave packet evolution," *Journal of Chemical Physics*, vol. 83, no. 10, pp. 5013–5018, 1985.

[5] D. J. Tannor, R. Kosloff, and S. A. Rice, "Coherent pulse sequence induced control of selectivity of reactions: exact quantum mechanical calculations," *Journal of Chemical Physics*, vol. 85, no. 10, pp. 5805–5820, 1986.

[6] M. Dantus and V. V. Lozovoy, "Experimental coherent laser control of physicochemical processes," *Chemical Reviews*, vol. 104, no. 4, pp. 1813–1860, 2004.

[7] K. Ohmori, "Wave-packet and coherent control dynamics," *Annual Review of Physical Chemistry*, vol. 60, no. 1, pp. 487–511, 2009.

[8] P. Tzallas, E. Skantzakis, L. A. Nikolopoulos, G. D. Tsakiris, and D. Charalambidis, "Extreme-ultraviolet pump-probe studies of one-femtosecond-scale electron dynamics," *Nature Physics*, vol. 7, no. 10, pp. 781–784, 2011.

[9] T. Okino, Y. Furukawa, Y. Nabekawa et al., "Direct observation of an attosecond electron wave packet in a nitrogen molecule," *Science Advances*, vol. 1, no. 8, article a1500356, 2015.

[10] S. Usenko, D. Schwickert, A. Przystawik et al., "Auger electron wave packet interferometry on extreme timescales with coherent soft x-rays," *Journal of Physics B*, vol. 53, no. 24, article 244008, 2020.

[11] S. Cavalieri, R. Eramo, M. Materazzi, C. Corsi, and M. Bellini, "Ramsey-type spectroscopy with high-order harmonics," *Physical Review Letters*, vol. 89, no. 13, article 133002, 2002.

[12] I. Liontos, S. Cavalieri, C. Corsi et al., "Ramsey spectroscopy of bound atomic states with extreme-ultraviolet laser harmonics," *Optics Letters*, vol. 35, no. 6, pp. 832–834, 2010.

[13] R. Eramo, S. Cavalieri, C. Corsi, I. Liontos, and M. Bellini, "Method for high-resolution frequency measurements in the extreme ultraviolet regime: random-sampling Ramsey spectroscopy," *Physical Review Letters*, vol. 106, no. 21, article 213003, 2011.

[14] L.-M. Koll, L. Maikowski, L. Drescher, M. J. J. Vrakking, and T. Witting, "Phase-locking of time-delayed attosecond XUV pulse pairs," *Optics Express*, vol. 30, no. 5, pp. 7082–7095, 2022.

[15] L. S. Dreissen, C. Roth, E. L. Gründeman, J. J. Krauth, M. Favier, and K. S. E. Eikema, "High-precision Ramsey-comb spectroscopy based on high-harmonic generation," *Physical Review Letters*, vol. 123, no. 14, article 143001, 2019.

[16] A. Wituschek, L. Bruder, E. Allaria et al., "Tracking attosecond electronic coherences using phase-manipulated extreme ultraviolet pulses," *Nature Communications*, vol. 11, no. 1, Article ID 883, 2020.

[17] A. Wituschek, L. Bruder, E. Allaria et al., "High-gain harmonic generation with temporally overlapping seed pulses and application to ultrafast spectroscopy," *Optics Express*, vol. 28, no. 20, pp. 29976–29990, 2020.

[18] Y. Hikosaka, T. Kaneyasu, M. Fujimoto, H. Iwayama, and M. Katoh, "Coherent control in the extreme ultraviolet and attosecond regime by synchrotron radiation," *Nature Communications*, vol. 10, no. 1, Article ID 4988, 2019.

[19] T. Kaneyasu, Y. Hikosaka, M. Fujimoto, H. Iwayama, and M. Katoh, "Electron wave packet interference in atomic inner-shell excitation," *Physical Review Letters*, vol. 126, no. 11, Article ID 113202, 2021.

[20] Y. Kobayashi, D. M. Neumark, and S. R. Leone, "Attosecond XUV probing of vibronic quantum superpositions in Br_2^+," *Physical Review A*, vol. 102, no. 5, article 051102(R), 2020.

[21] Y. Nabekawa, T. Shimizu, T. Okino et al., "Interferometric autocorrelation of an attosecond pulse train in the single-cycle regime," *Physical Review Letters*, vol. 97, no. 15, Article ID 153904, 2006.

[22] T. Matsubara, S. Fukahori, E. Lötstedt, Y. Nabekawa, K. Yamanouchi, and K. Midorikawa, "300 attosecond

response of acetylene in two-photon ionization/dissociation processes," *Optica*, vol. 8, no. 8, pp. 1075–1083, 2021.

[23] T. Nishi, E. Lötstedt, and K. Yamanouchi, "Entanglement and coherence in photoionization of H_2 by an ultrashort XUV laser pulse," *Physical Review A*, vol. 100, no. 1, article 013421, 2019.

[24] M. J. J. Vrakking, "Control of attosecond entanglement and coherence," *Physical Review Letters*, vol. 126, no. 11, Article ID 113203, 2021.

[25] L.-M. Koll, L. Maikowski, L. Drescher, T. Witting, and M. J. J. Vrakking, "Experimental control of quantum-mechanical entanglement in an attosecond pump-probe experiment," *Physical Review Letters*, vol. 128, no. 4, article 043201, 2022.

[26] Y. Nabekawa, A. A. Eilanlou, Y. Furukawa, K. L. Ishikawa, H. Takahashi, and K. Midorikawa, "Multi-terawatt laser system generating 12-fs pulses at 100 Hz repetition rate," *Applied Physics B: Lasers and Optics*, vol. 101, no. 3, pp. 523–534, 2010.

[27] Y. Nabekawa, T. Shimizu, Y. Furukawa, E. J. Takahashi, and K. Midorikawa, "Interferometry of attosecond pulse trains in the extreme ultraviolet wavelength region," *Physical Review Letters*, vol. 102, no. 21, Article ID 213904, 2009.

[28] M. Huppert, I. Jordan, and H. J. Wörner, "Attosecond beamline with actively stabilized and spatially separated beam paths," *Review of Scientific Instruments*, vol. 86, Article ID 123106, 2015.

[29] P. Balcou, P. Salières, A. L'Huillier, and M. Lewenstein, "Generalized phase-matching conditions for high harmonics: the role of field-gradient forces," *Physical Review A*, vol. 55, no. 4, pp. 3204–3210, 1997.

[30] Y. Nabekawa, Y. Furukawa, T. Okino et al., "Settling time of a vibrational wavepacket in ionization," *Nature Communications*, vol. 6, no. 1, Article ID 213904, 2015.

[31] G. A. Garcia, L. Nahon, and I. Powis, "Two-dimensional charged particle image inversion using a polar basis function expansion," *Review of Scientific Instruments*, vol. 75, no. 11, pp. 4989–4996, 2004.

[32] K. L. Ishikawa and K. Midorikawa, "Above-threshold double ionization of helium with attosecond intense soft x-ray pulses," *Physical Review A*, vol. 72, no. 1, article 013407, 2005.

[33] K. L. Ishikawa and K. Ueda, "Competition of resonant and nonresonant paths in resonance-enhanced two-photon single ionization of He by an ultrashort extreme-ultraviolet pulse," *Physical Review Letters*, vol. 108, no. 3, article 033003, 2012.

[34] K. Ishikawa and K. Ueda, "Photoelectron angular distribution and phase in two-photon single ionization of H and he by a femtosecond and attosecond extreme-ultraviolet pulse," *Applied Sciences*, vol. 3, no. 1, pp. 189–213, 2013.

[35] M. D. Fraia, O. Plekan, C. Callegari et al., "Complete characterization of phase and amplitude of bichromatic extreme ultraviolet light," *Physical Review Letters*, vol. 123, no. 21, Article ID 213904, 2019.

[36] V. Stooß, M. Hartmann, P. Birk et al., "XUV-beamline for attosecond transient absorption measurements featuring a broadband common beam-path time-delay unit and in situ reference spectrometer for high stability and sensitivity," *Review of Scientific Instruments*, vol. 90, no. 5, article 053108, 2019.

[37] A. Kramida, Y. Ralchenko, J. Reader, and NIST ASD Team, *NIST Atomic Spectra Database (ver. 5.8)*, National Institute of Standards and Technology, Gaithersburg, MD, 2020, https://physics.nist.gov/asd.

[38] T. Bredtmann, S. Chelkowski, and A. D. Bandrauk, "Monitoring attosecond dynamics of coherent electron-nuclear wave packets by molecular high-order-harmonic generation," *Physical Review A*, vol. 84, no. 2, article 021401(R), 2011.

[39] G. J. Halász, A. Perveaux, B. Lasorne, M. A. Robb, F. Gatti, and Á. Vibók, "Coherence revival during the attosecond electronic and nuclear quantum photodynamics of the ozone molecule," *Physical Review A*, vol. 88, no. 2, article 023425, 2013.